

Supporting Information

Enantioselective separation in humid conditions by chiral Hofmann Clathrates: new opportunities for vintage materials

Ekaterina Mamontova,^a Philippe Trens,^b Fabrice Salles,^c Bernard Fraisse,^c Olinda Gimello,^b Yannick Guari,^a and Joulia Larionova,^a and Jérôme Long^{*a}

a. Institut Charles Gerhardt, Equipe Ingénierie Moléculaire et Nano-Objets, Université de Montpellier, ENSCM, CNRS. Place Eugène Bataillon, 34095 Montpellier Cedex 5, France, E-mail : jerome.long@umontpellier.fr

b. Institut Charles Gerhardt, Equipe Matériaux Avancés pour la Catalyse et la Santé, ENSCM, CNRS, Université de Montpellier, 240 Avenue du Professeur Emile Jeanbreau, 34090 Montpellier, France

c. Institut Charles Gerhardt, Equipe Agrégats, Interfaces et Matériaux pour l'Energie, Université de Montpellier, ENSCM, CNRS. Place Eugène Bataillon, 34095 Montpellier Cedex 5, France

Table of Contents

Figure S1. Photographs of powdered 1, R-1, S-1 and (+/-)-1.....	3
Figure S2. IR spectra of 1 (left) and comparison between IR spectra of 1, R and R-1 (right).	3
Figure S3. IR spectra of 1 (black), R-1 (blue), S-1 (red) and (+/-)-1 (green).	3
Figure S4. Top: TGA analysis obtained with a $5^{\circ}\text{C}.\text{min}^{-1}$ heating rate for 1 (black), R-1 (blue), S-1 (red) and (+/-)-1 (green). Bottom: Magnification in the low temperature region for R-1 (blue), S-1 (red) showing the two water losses. The dashed lines account for the first derivative	4
Figure S5. Le Bail refinements for 1, R-1, S-1 and (+/-)-1.	5
Table S1. Crystallographic Data.	6
Figure S6. Structures for R-1 and S-1 from periodic DFT calculations using the experimental unit cell parameters, for an alternate ligands repartition and for aligned sequence considering unit cell composed by two layers	7
Table S2. Energy values obtained from geometry optimization by DFT for the different distributions of the ligands in R-1 and S-1	7
Figure S7. Analysis of the strongest interactions in the empty R-1 for two arrangements of the ligands ((a) and (b)) and S-1 (c) structures from DFT calculations	8
Figure S8. IR spectra of R-1 before and after activation at 100°C under vacuum.	9
Figure S9. Solid-state CD spectra of R-1 before (blue) and after (magenta) activation at 100°C under vacuum.	9
Figure S10. Adsorption/desorption isotherms of H_2O and (+/-)-BuOH in the racemic (+/-)-1 clathrate.....	10
Figure S11. Adsorption/desorption isotherms of H_2O with 1 and (+/-)-1 clathrate.....	10
Figure S12. Nitrogen adsorption isotherms.	11
Figure S13. Adsorption/desorption isotherms of H_2O (a) and (+/-)-BuOH (b) in the racemic (+/-)-1 and R-1 clathrates.	12
Figure S14. Chromatogram of (+/-)-BuOH, R-BuOH and S-BuOH (acetonitrile:water 70:30) using the chiral R-1 clathrate.....	13
Figure S15. Interactions in the highest energetical conformations between R-BuOH (a) and S-BuOH (b) with R-phenylethylamine ligand from DFT calculations.	14
Figure S16. Partial charges for R-BuOH (a) and S-BuOH (b) molecules extracted from DFT calculations.	14
Figure S17. Plausible configurations for the interactions between R-BuOH and S-BuOH with R-1 ligands from Monte Carlo calculations in the co-adsorption case. Snapshots (a) and (b) correspond to the interaction of R-BuOH and S-BuOH respectively in R-1 where all the ligands are on the same face of the layers, while (c) and (d) correspond to the interaction of R-BuOH and S-BuOH respectively in R-1 where all the ligands are alternated regarding the layers.....	15



Figure S1. Photographs of powdered **1**, ***R*-1**, ***S*-1** and **(+/-)-1**.

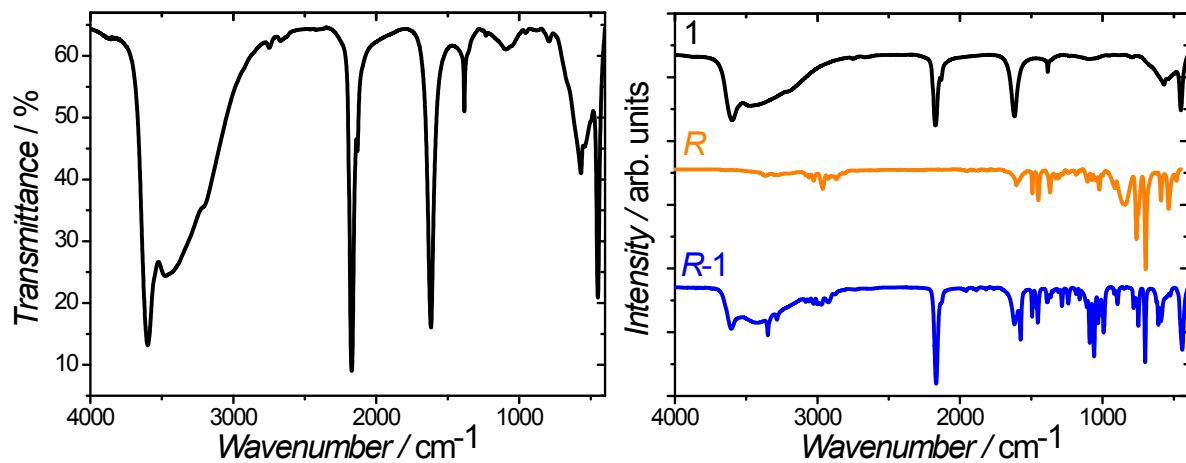


Figure S2. IR spectra of **1** (left) and comparison between IR spectra of **1**, ***R*** and ***R*-1** (right).

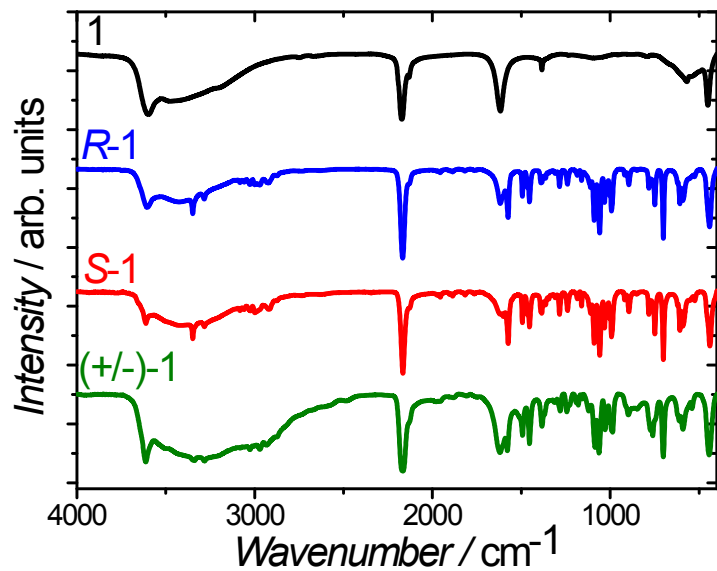


Figure S3. IR spectra of **1** (black), ***R*-1** (blue), ***S*-1** (red) and **(+/-)-1** (green).

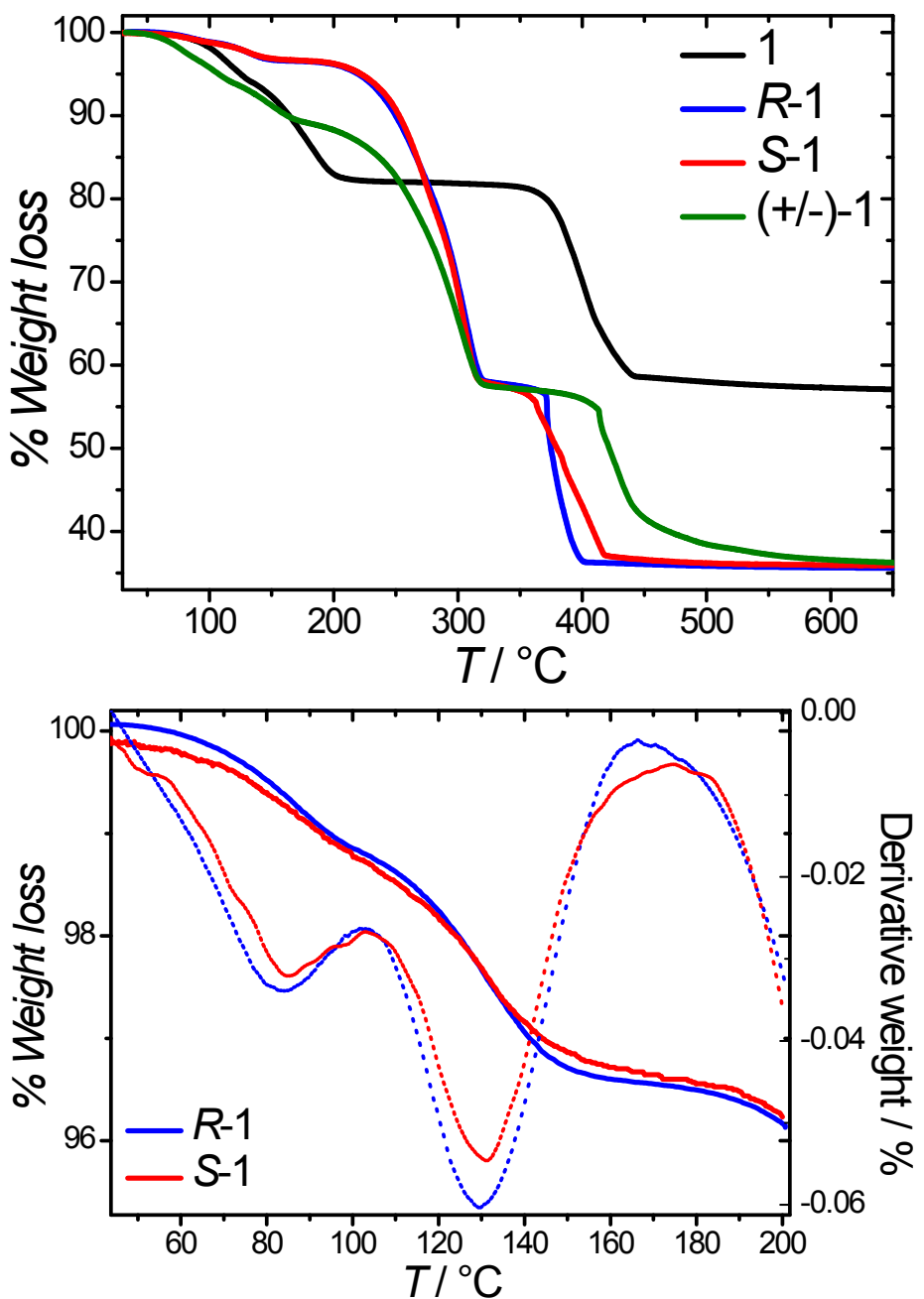
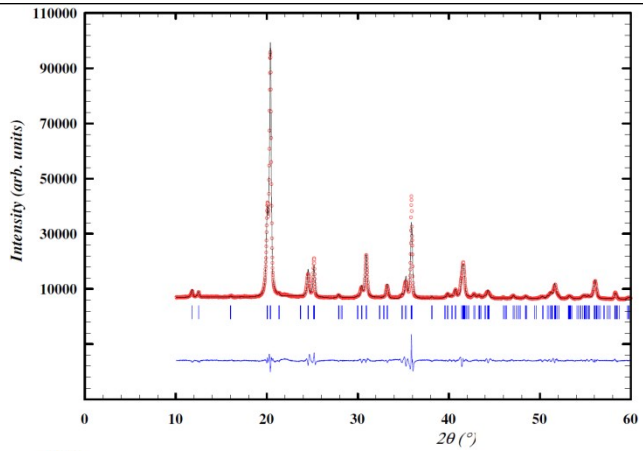
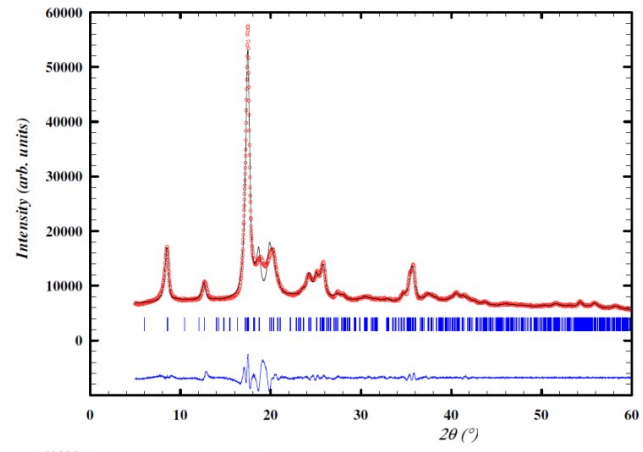


Figure S4. Top: TGA analysis obtained with a $5\text{ }^{\circ}\text{C}.\text{min}^{-1}$ heating rate for **1** (black), **R-1** (blue), **S-1** (red) and **(+/-)-1** (green). Bottom: Magnification in the low temperature region for **R-1** (blue), **S-1** (red) showing the two water losses. The dashed lines account for the first derivative

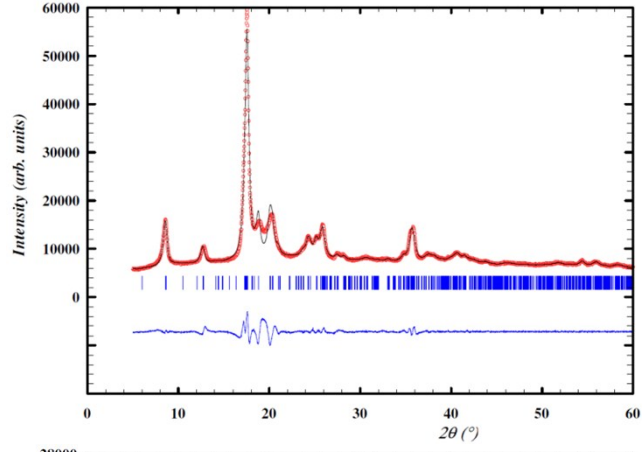
1



R-1



S-1



(+/-)-1

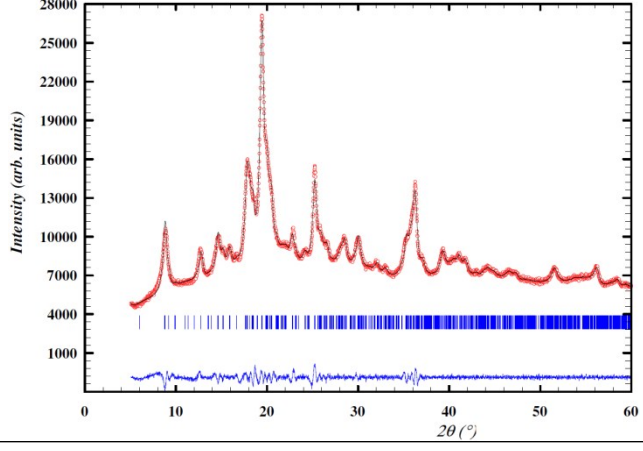


Figure S5. Le Bail refinements for **1**, **R-1**, **S-1** and **(+/-)-1**.

Table S1. Crystallographic Data.

	1	R-1	S-1	(+/-)-1
Formula	Ni ₂ C ₄ N ₄ H ₇ O _{3.5}	Ni ₂ C _{15.2} N _{5.4} H _{17.2} O _{0.9}	Ni ₂ C _{15.2} N _{5.4} H _{17.2} O _{0.9}	Ni ₂ C _{15.2} N _{5.4} H _{17.2} O _{0.9}
Temperature (K)	295	295	295	295
2θ Range for Data Collection (°)	4-60	4-60	4-60	4-60
Crystal System	orthorhombic	monoclinic	monoclinic	monoclinic
Space Group	<i>Ima2</i>	<i>P2</i>	<i>P2</i>	<i>P2/m</i>
<i>a</i>	14.157(2)	7.068(3)	7.014(3)	14.879(3)
<i>b</i>	8.860(1)	14.703(5)	14.674(1)	9.611(4)
<i>c</i> (Å)	7.071(1)	10.430(3)	10.335(5)	10.169(5)
α	90.00	90.00	90.00	90.00
β	90.00	98.16(2)	97.81(5)	98.17(2)
γ (°)	90.00	90.00	90.00	90.00

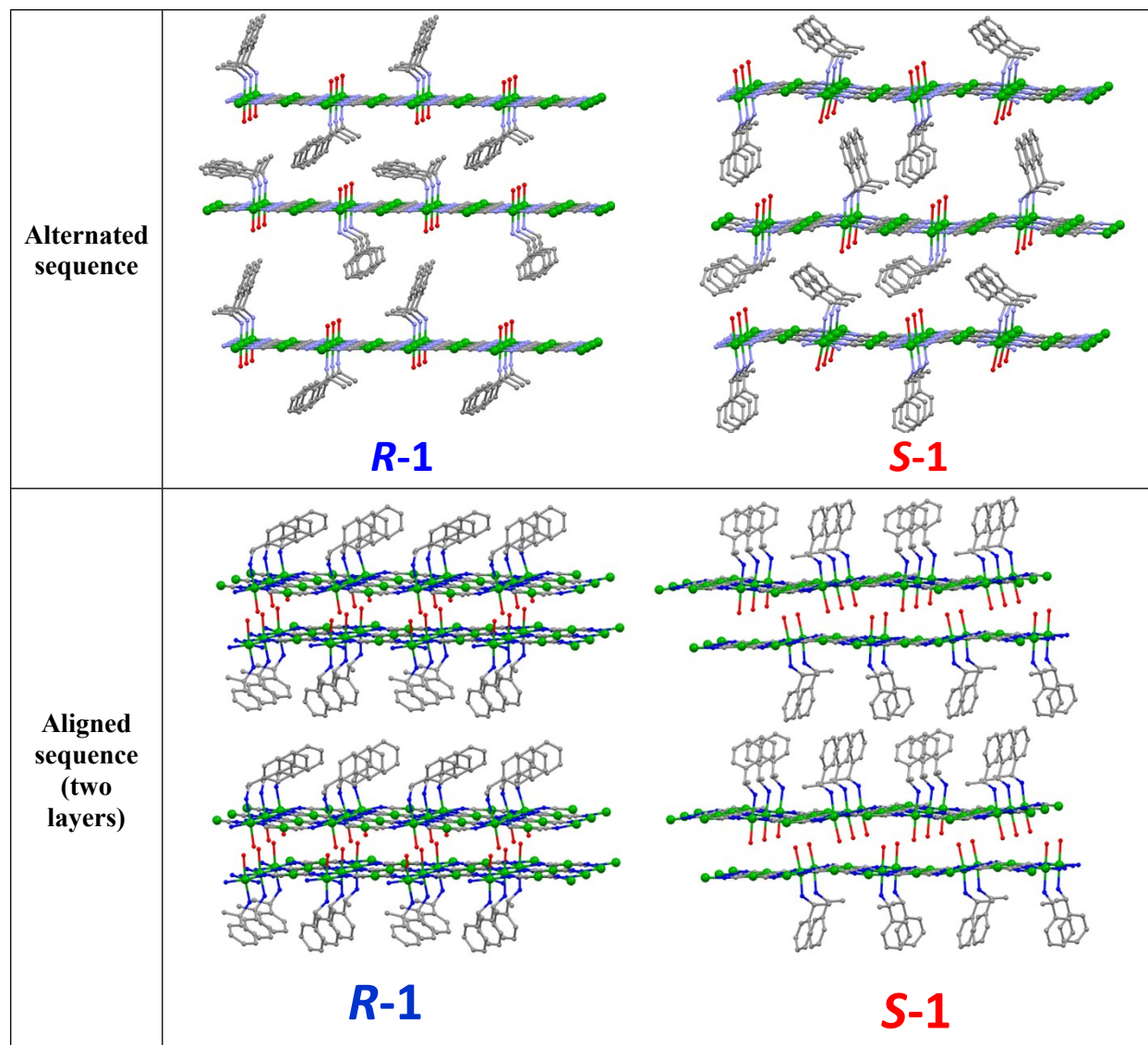


Figure S6. Structures for **R-1** and **S-1** from periodic DFT calculations using the experimental unit cell parameters, for an alternate ligands repartition and for aligned sequence considering unit cell composed by two layers

Table S2. Energy values obtained from geometry optimization by DFT for the different distributions of the ligands in **R-1** and **S-1**

Structures	Energy (in Ha)
R-1 with all ligands aligned in the same direction	-15325.4538208
R-1 with alternated ligands	-15325.4287967
R-1 with aligned ligands (two layers)	-15325.4445678
S-1 with all ligands aligned in the same direction	-15325.4307791
S-1 with alternated ligands on the two faces	-15325.4246970
S-1 with aligned ligands (two layers)	-15325.4284003

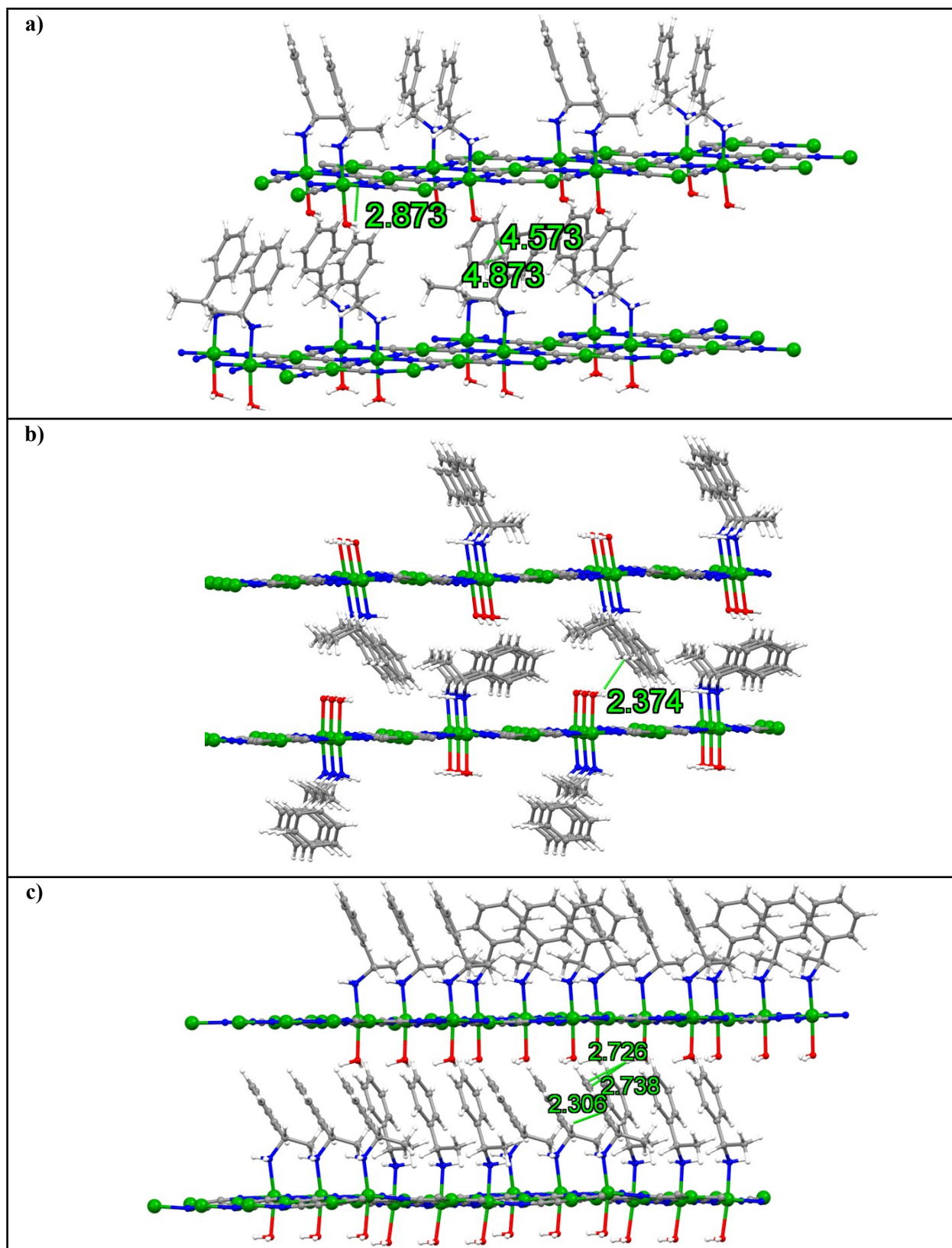


Figure S7. Analysis of the strongest interactions in the empty *R*-1 for two arrangements of the ligands ((a) and (b)) and *S*-1 (c) structures from DFT calculations

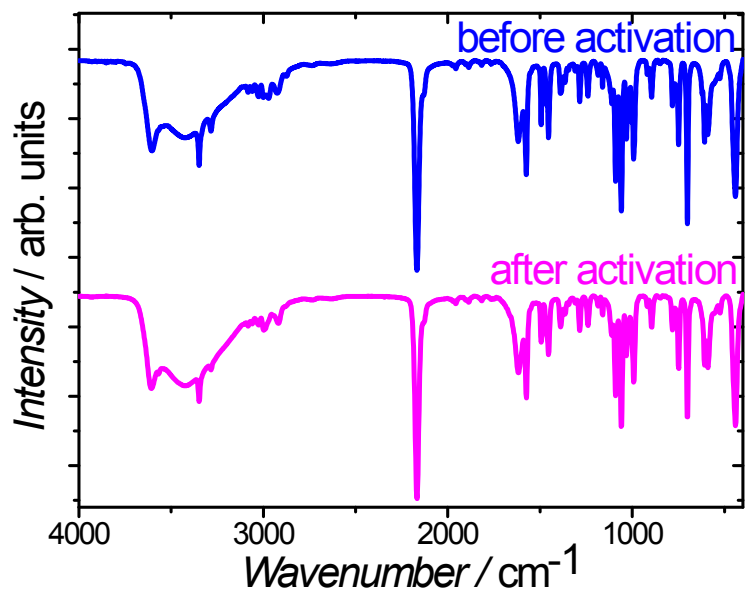


Figure S8. IR spectra of *R*-1 before and after activation at 100°C under vacuum.

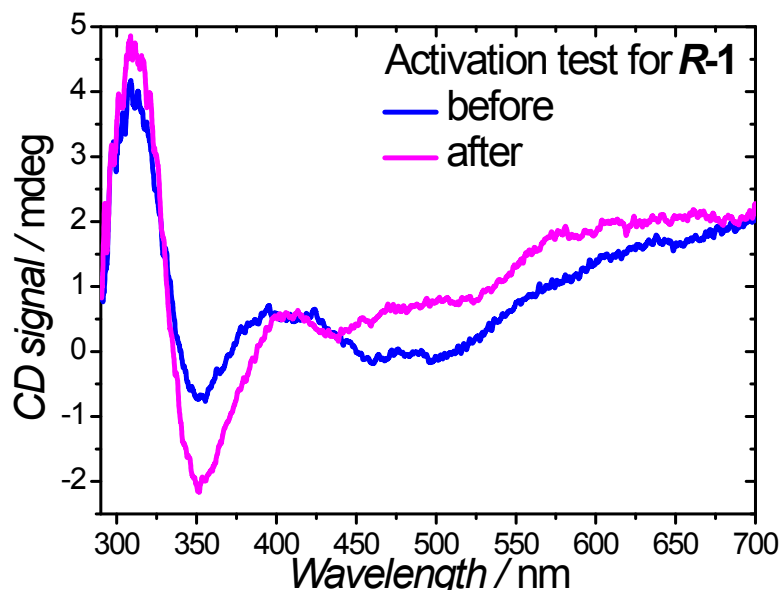


Figure S9. Solid-state CD spectra of *R*-1 before (blue) and after (magenta) activation at 100°C under vacuum.

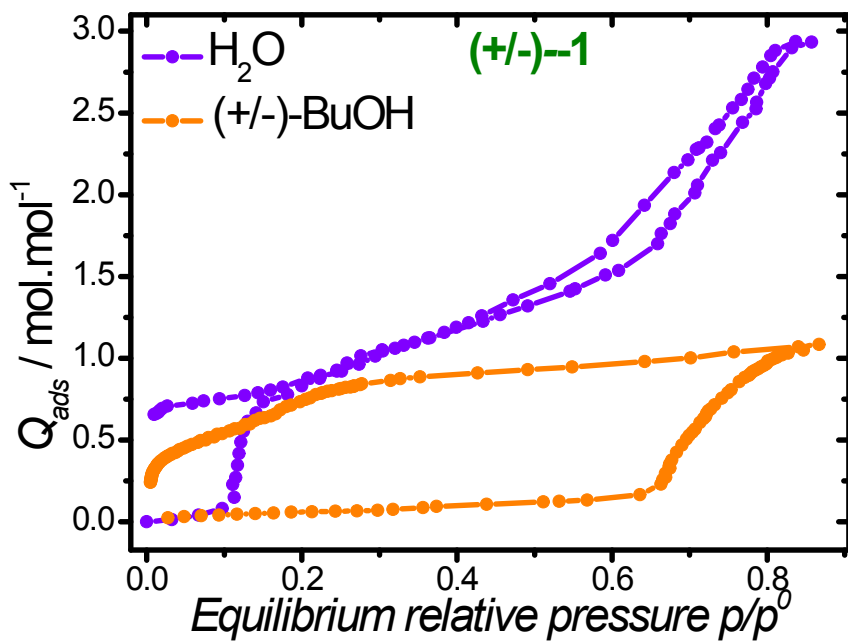


Figure S10. Adsorption/desorption isotherms of H_2O and $(+/-)$ -BuOH in the racemic $(+/-)\text{-1}$ clathrate.

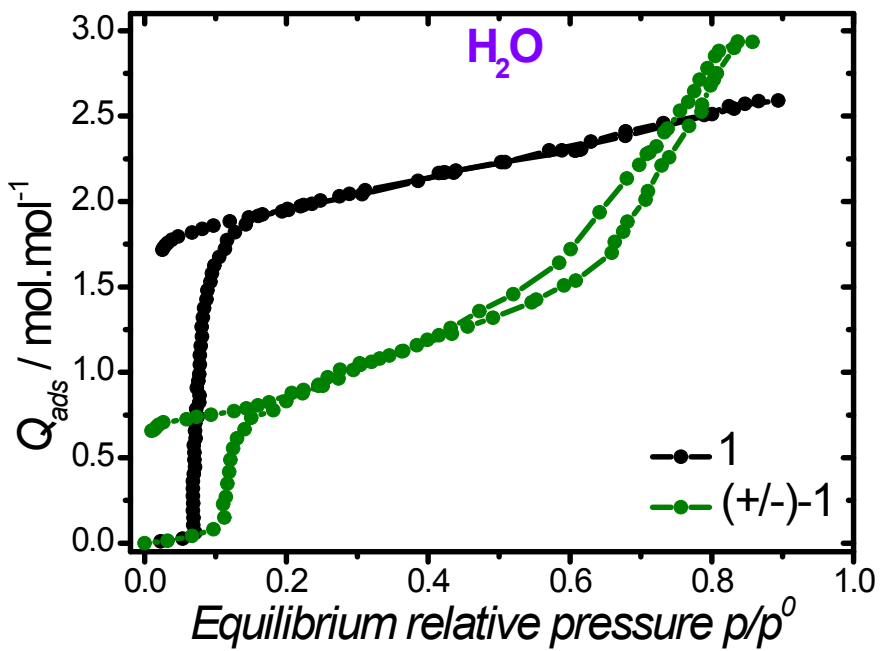


Figure S11. Adsorption/desorption isotherms of H_2O with **1** and $(+/-)\text{-1}$ clathrate.

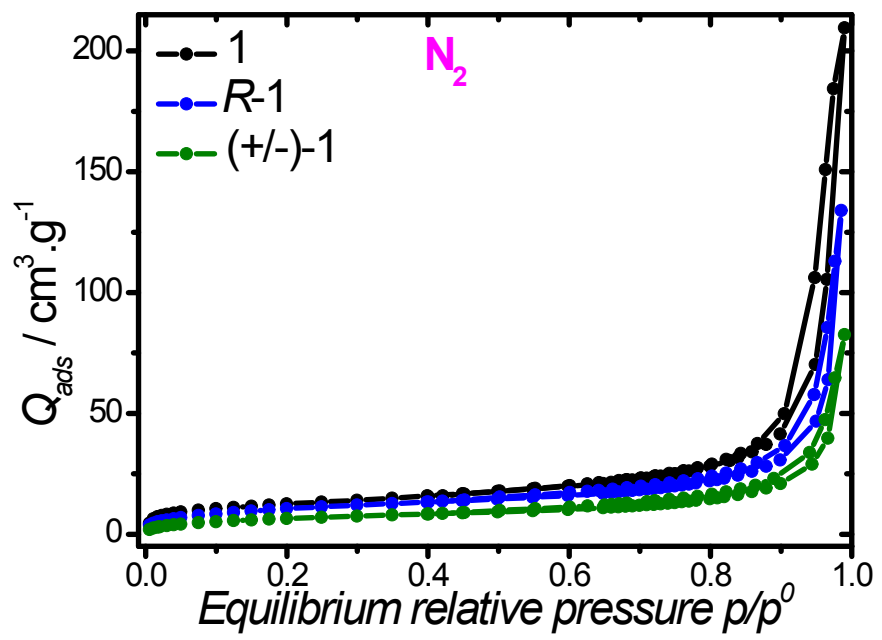


Figure S12. Nitrogen adsorption isotherms.

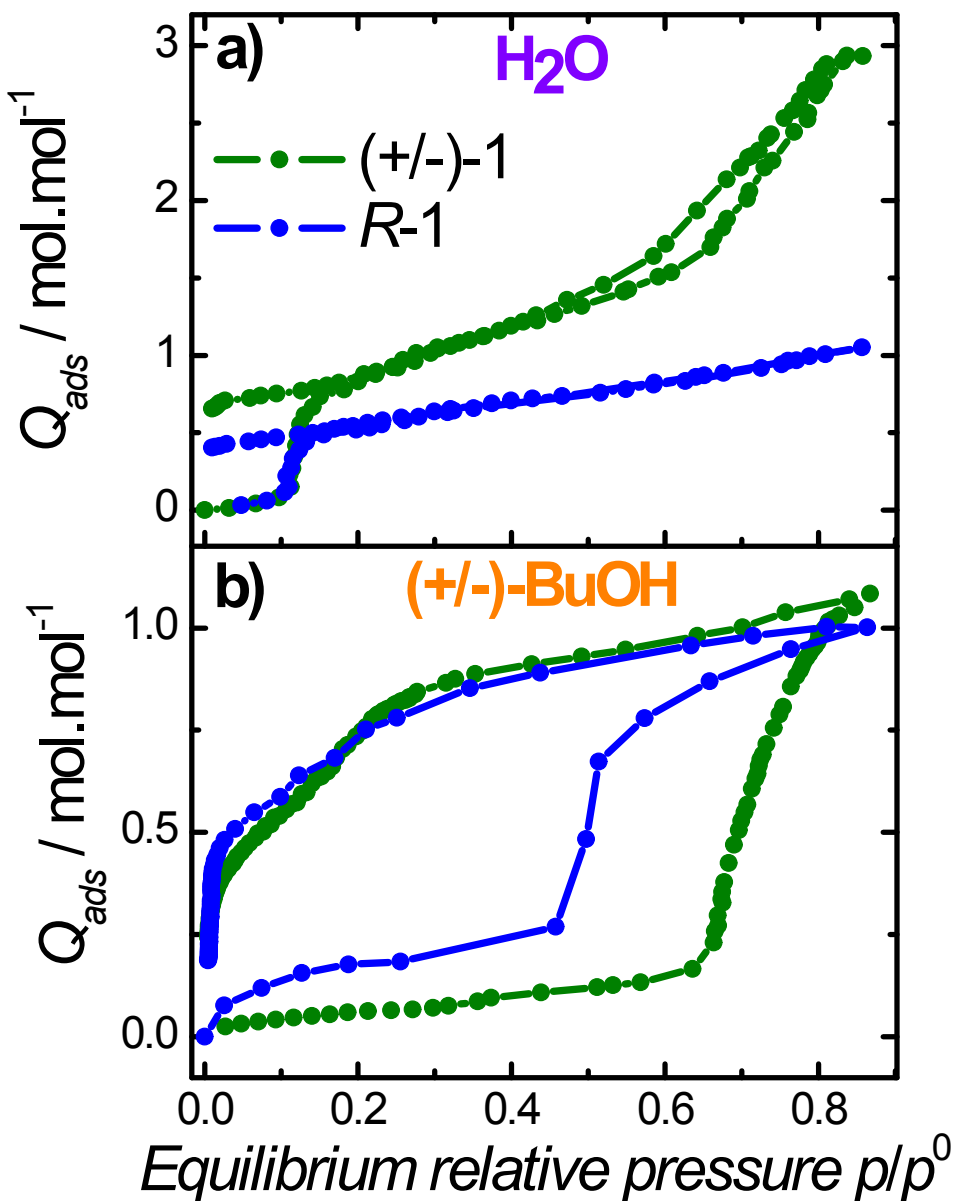


Figure S13. Adsorption/desorption isotherms of H_2O (a) and $(+/-)$ - BuOH (b) in the racemic $(+/-)$ -**1** and **R-1** clathrates.

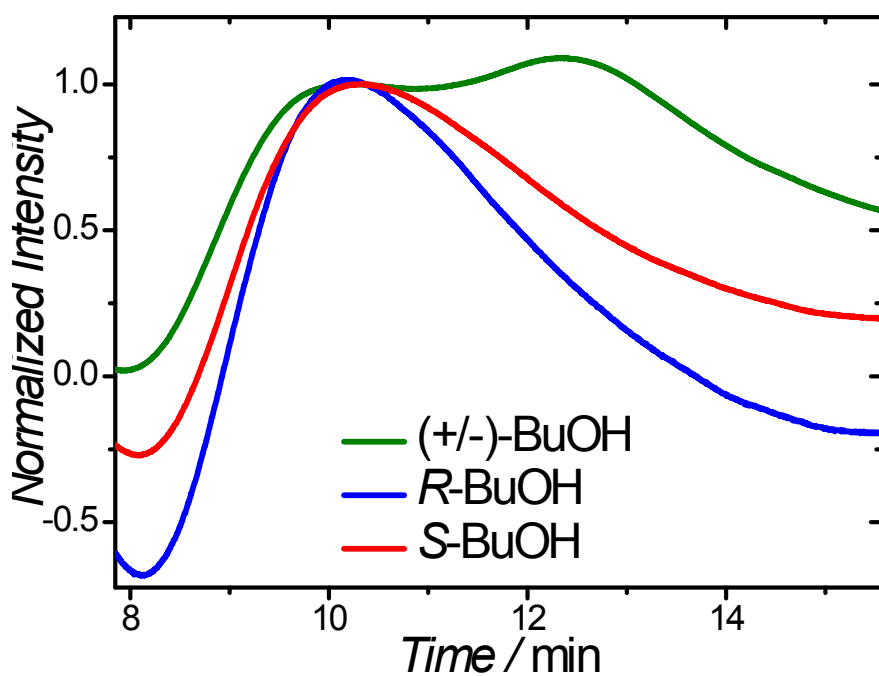


Figure S14. Chromatogram of $(+/-)$ -BuOH, R -BuOH and S -BuOH (acetonitrile:water 70:30) using the chiral R -**1** clathrate.

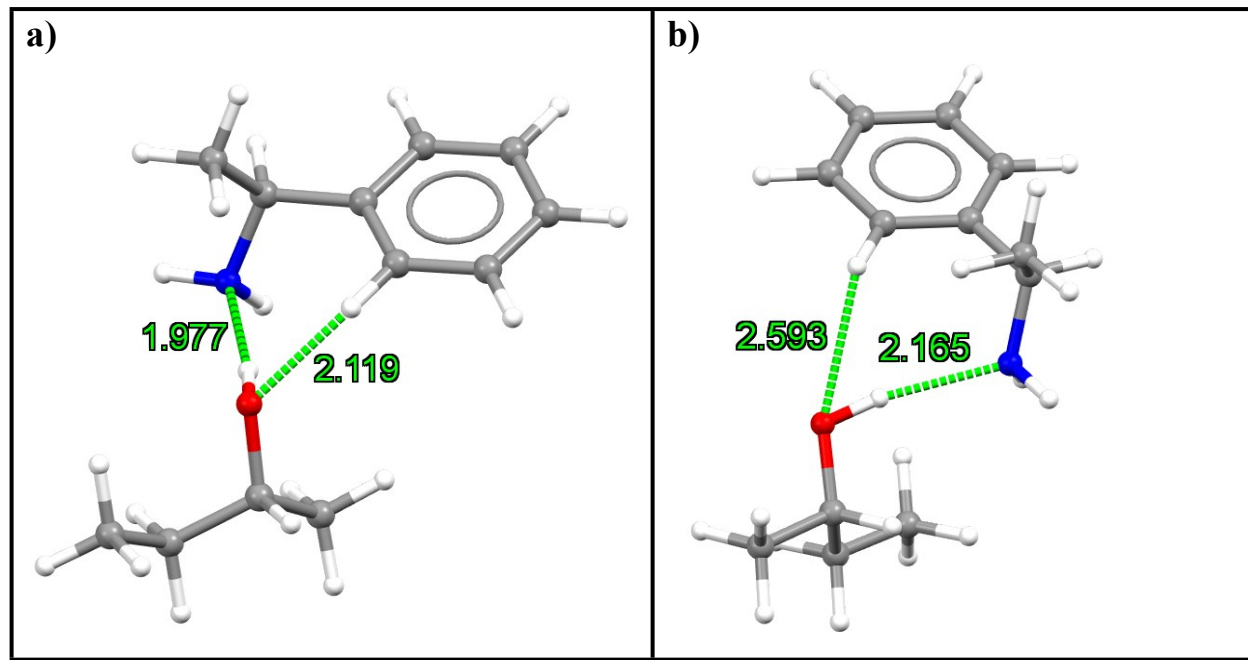


Figure S15. Interactions in the highest energetical conformations between *R*-BuOH (a) and *S*-BuOH (b) with *R*-phenylethylamine ligand from DFT calculations.

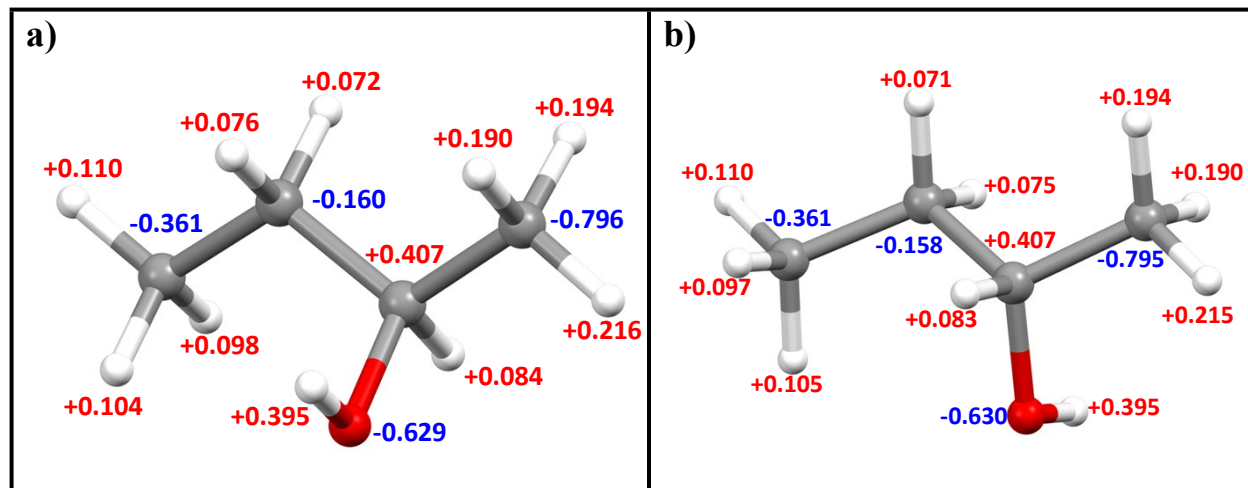


Figure S16. Partial charges for *R*-BuOH (a) and *S*-BuOH (b) molecules extracted from DFT calculations.

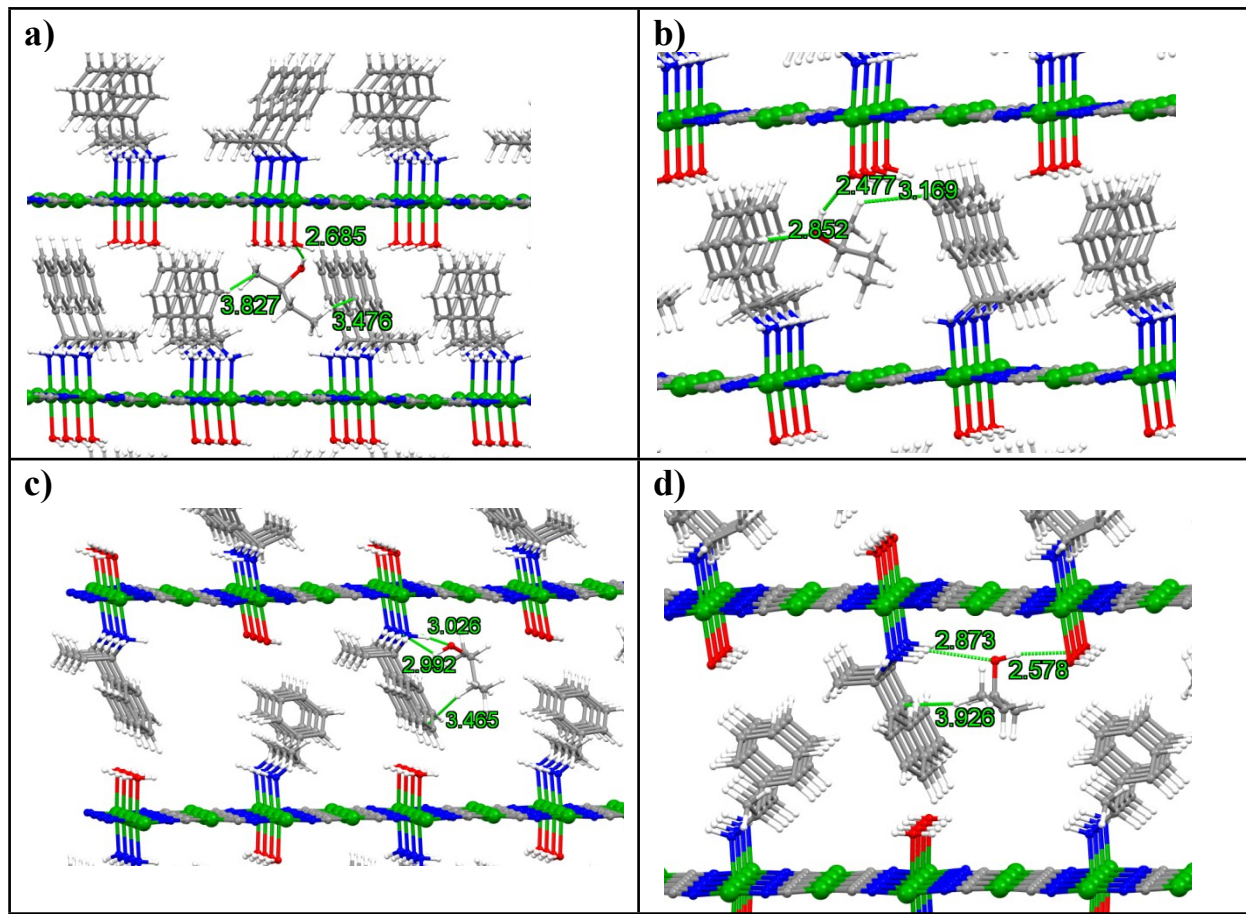


Figure S17. Plausible configurations for the interactions between *R*-BuOH and *S*-BuOH with **R-1** ligands from Monte Carlo calculations in the co-adsorption case. Snapshots (a) and (b) correspond to the interaction of *R*-BuOH and *S*-BuOH respectively in **R-1** where all the ligands are on the same face of the layers, while (c) and (d) correspond to the interaction of *R*-BuOH and *S*-BuOH respectively in **R-1** where all the ligands are alternated regarding the layers.